Jens Kleinjung[1]*
Marie-Christine Petit[1]
Piotr Orlewski[1]
Avgi Mamalaki[2]
Socrates J. Tzartos[2]
Vassilios Tsikaris[3]
Maria Sakarellos-Daitsiotis[3]
Constantinos Sakarellos[3]
Michel Marraud[1]
Manh-Thong Cung[1]
[1] *Laboratoire de Chimie-Physique Macromoleculaire, UMR 7568 CNRS-INPL, ENSIC, BP 451, 54001 Nancy Cedex, France*

[2] *Department of Biochemistry, Hellenic Pasteur Institute, 127 Vassilissis Sofias Avenue, 115 21 Athens, Greece*

[3] *Department of Chemistry, University of Ioannina, Box 1186, 451 10 Ioannina, Greece*

Received 29 October 1998; accepted 15 December 1998

The Third-Dimensional Structure of the Complex Between an Fv Antibody Fragment and an Analogue of the Main Immunogenic Region of the Acetylcholine Receptor: A Combined Two-Dimensional NMR, Homology, and Molecular Modeling Approach

Abstract: *Binding of autoantibodies to the acetylcholine receptor (AChR) plays a major role in the autoimmune disease* Myasthenia gravis *(MG). In this paper, we propose a structure model of a putative immunocomplex that gives rise to the reduction of functional AChR molecules during the course of MG. The model complex consists of the [G^{70}, Nle^{76}] decapeptide analogue of the main immunogenic region (MIR), representing the major antigenic epitope of AChR, and the single chain Fv fragment of monoclonal antibody 198, a potent MG autoantibody. The structure of the complexed decapeptide antigen [G^{70}, Nle^{76}]MIR was determined using two-dimensional nmr, whereas the*

* *Present address:* Division of Physical Biochemistry, National Institute for Medical Research, The Ridgeway, Mill Hill, London NW7 1AA, United Kingdom

Correspondence to: M.-T. Cung

Contract grant sponsor: Association Française contre les Myopathies, CNRS, and EU

Contract grant number: CT94-0547 (EU)

Biopolymers, Vol. 53, 113–128 (2000)

CCC 0006-3525/00/020113-16

antibody structure was derived by means of homology modeling. The final complex was constructed using calculational docking and molecular dynamics. We termed this approach "directed modeling," since the known peptide structure directs the prestructured antibody binding site to its final conformation. The independently derived structures of the peptide antigen and antibody binding site already showed a high degree of surface complementarity after the initial docking calculation, during which the peptide was conformationally restrained. The docking routine was a soft algorithm, applying a combination of Monte Carlo simulation and energy minimization. The observed shape complementarity in the docking process suggested that the structure assessments already led to anti-idiotypic conformations of peptide antigen and antibody fragment. Refinement of the complex by dynamic simulation yielded improved surface adaptation by small rearrangements within antibody and antigen. The complex presented herein was analyzed in terms of antibody–antigen interactions, properties of contacting surfaces, and segmental mobility. The structural requirements for AChR complexation by autoantibodies were explored and compared with experimental data from alanine scans of the MIR peptides. The analysis revealed that the N-terminal loop of the peptide structure, which is indispensable for antibody recognition, aligns three hydrophobic groups in a favorable arrangement leading to the burial of 40% of the peptide surface in the binding cleft upon complexation. These data should be valuable in the rational design of an Fv mutant with much improved affinity for the MIR and AChR to be used in therapeutic approaches in MG. © 2000 John Wiley & Sons, Inc. Biopoly 53: 113–128, 2000

Keywords: *anti-acetylcholine receptor single chain Fv antibody; homology modeling; molecular dynamics;* Myasthenia gravis*; protein structure prediction; transferred nuclear Overhauser effect spectroscopy; docking*

INTRODUCTION

Myasthenia gravis (MG) is a neuromuscular disease induced by autoantibodies that are raised against the acetylcholine receptor (AChR),[1] a ligand-gated membrane glycoprotein composed of five homologous subunits of the stoichiometry $\alpha_2\beta\gamma\delta$ or $\alpha_2\beta\epsilon\delta$.[2] Previous investigations have shown that two thirds of the anti-AChR antibodies found in patients or in immunized rats are directed against a small region of the AChR sequence, named the "main immunogenic region" (MIR).[1,3,4] A major part of the MIR has been localized between residues 67–76 of the AChR α-subunit. The α67–76 sequence is W^{67}–N^{68}–P^{69}–A^{70}–D^{71}–Y^{72}–G^{73}–G^{74}–I^{75}–K^{76} in *Torpedo* electric organ AChR and W^{67}–N^{68}–P^{69}–D^{70}–D^{71}–Y^{72}–G^{73}–G^{74}–V^{75}–K^{76} in human muscle AChR, with one nonconservative (α70) and one conservative (α75) substitution.[3,4] Structural studies in solution revealed essential sequential and structural characteristics of different MIR peptide analogues.[5] Sequence alanine scanning revealed the important roles of residues N^{68}, P^{69}, and D^{71} in the recognition process, since substitution of any one of these residues greatly impaired antibody binding.[6–8] In addition, the N-terminal β-turn conformation was shown to be an indispensable structural motif with regard to antibody recognition.[5,9] Despite the considerable insight into the biological function of various MIR peptide analogues and anti-MIR antibodies, little is reported about the structural aspects of the immunocomplex. An improved understanding of immunogenicity can be obtained by a study at the atomic level.

The aim of this study was the construction of a model of the immunocomplex between MIR analogue and anti-AChR autoantibodies so that these data may be used for the rational design of a high affinity therapeutic antibody fragment. We analyzed the structure of the [G^{70}, Nle^{76}]MIR decapeptide, a Torpedo MIR analogue which has about twofold enhancement of binding capacity to mAb198 in comparison with the human MIR analogue, complexed to the antibody fragment single chain Fv198 (scFv198) by means of two-dimensional (2D) nmr and molecular modeling while the antibody structure was constructed by means of homology modeling and de novo design. Following the description of variable antibody domains[10] and the conformational analysis of the canonical structures,[11] the increase in the number of published antibody structures[12,13] has led to the successful prediction of antibody structures.[14] In most approaches, reported antibody structures were used as templates,[14–20] whereas de novo approaches were rarely undertaken.[21–23] Moreover, accurate knowledge-based prediction of binding sites was feasible when the structure of the antigen and the sequence of the antibody are known.

The scFv198 fragment consists of the variable domains of the heavy and light antibody chains of the mAb198 joined by a flexible 15-residue linker. The peptide was then docked using Monte Carlo simulations (MC) to an antibody model of scFv198 that was

constructed beforehand on the basis of template structures. The model complex revealed key features for the interaction and structural requirements for the conformation of antigenic MIR peptides.

MATERIALS AND METHODS

Materials

The mAb198 was obtained from rats immunized with human AChR.[3] The preparations used were obtained from serum-free hybridoma supernatants, concentrated by Amicon ultrafiltration and dialyzed against phosphate-buffered saline containing 0.05% sodium azide. The production and characteristics of the mAb have been described earlier.[3,4,7] Bacterial expression and sequencing of the scFv fragment of anti-AChR mAb198 have been reported elsewhere.[24] [G^{70}, Nle^{76}]MIR was synthesized using standard solid-phase peptide chemistry on phenyl acetamido methyl (PAM) resin. Synthesis was performed by Boc strategy with usual side-chain protection. The peptide was deprotected and cleaved from the resin by treatment with hydrogen fluoride. Final purification was achieved by reverse phase high performance liquid chromatography using an acetonitrile/water gradient.

NMR Experiments

Perdeuterated solvent D_2O (99.8% D) and internal standard sodium trimethylsilyl-3-propioniate 2,2,3,3-d_4 were purchased from the Commissariat à l'Energie Atomique (France). The MIR peptide and the mAb198 were dissolved in 0.1*M* phosphate buffer adjusted to pH 7.2, containing a mixture of H_2O/D_2O (9/1, v/v). The concentration of the peptide was 10 m*M* and the molar ratio of peptide to mAb198 was 50/1 in order to obtain the most intense TR-NOESY cross peak without spin diffusion. Spectra were recorded using a Bruker DRX-400 NMR spectrometer. Sample temperature was kept at 4°C during the nmr experiments. The 2D total correlated spectroscopy (TOCSY) and 2D-NOESY experiments were recorded in the pure-phase absorption mode with quadrature detection in both dimensions using the states time proportional phase incrementation mode.[25] Five mixing times of 100–500 ms were initially applied to derive the optimal mixing time interval avoiding spin diffusion. Selective water resonance suppression in the TOCSY and NOESY experiments was achieved by the WATERGATE sequence.[26,27] Data processing was performed on a Silicon Graphics workstation using Bruker-UXNMR software. Spectra analysis and resonance attribution were achieved by using the XEASY program.[28] The interproton distances were calculated from the NOESY cross-peak volumes by assuming isotropic motion with a single correlation time τ_c for all interacting spins. Distance calculations were calibrated by the cross peak volume of the β geminal protons of N^{68}, which are separated by 1.78 Å. A set of 73 interproton distance constraints was deduced from the NOESY spectrum (mixing time τ_m of 200 ms).

Methods of Computation

All calculations, i.e., distance geometry (DG), molecular dynamics (MD), docking calculations, and energy minimization (EM) were performed on an Indy Silicon Graphics workstation using BIOSYM software. For MD and EM calculations, the module DISCOVER_3 was used. The consistent-valence force field[29] with a default cutoff distance of 9.5 Å and a dielectric constant of 1 was applied to all molecules and fragments if not stated explicitly. MD calculations were performed in vacuo at 300 K with a step width of 1 fs after an initial heating phase of 5 ps for the peptides and 50 ps for the antibody complex. Electrical point charges of ionic residues were decreased by reducing the partial charge of atoms involved to half of their initial value. The purpose of the reduction was impairment of structural artifacts by overestimation of Coulomb interactions in vacuo. Stereochemical quality of all structures was assessed using the PROCHECK program.[30]

Peptide Conformation

DG calculations were executed using the programs DIANA and DYANA.[31,32] A set of 17 backbone–backbone, 36 backbone–side-chain, and 20 side-chain–side-chain distance restraints was implemented in the calculations. Angles ϕ of nonglycine and nonproline residues were fixed between $-5°$ and $-175°$ in order to suppress right-handed turns. A set of 150 random structures was generated and annealed in 10000 steps from temperature 8 to 0 units, measured in target function units. All DG calculations were performed using standard parameters. Structures were clustered into families and evaluated with regard to their stereochemical qualities. Clustering yielded a family of 72 structures exhibiting backbone rms deviations of 0.82 ± 0.36 Å. Each of the structures was submitted to 500 steps of minimization and 35 ps of MD at 300 K applying derived nmr restraints with a force constant of 4 kcal mol^{-1} $Å^{-2}$. Conjugate gradient EM was completed within 750 steps and final 50 iterations were performed without any restraints to relieve accidental atomic overlaps. Again, refined structures were clustered into families and analyzed as described above. One family of five structures showing internal backbone rms differences of 0.53 ± 0.16 Å appeared to be the most consistent in terms of energy contributions, stereochemical quality, and extent of agreement with experimental data.

Antibody Framework Structure Generation

Atomic coordinates of a Fv human immunoglobulin Pot IgM,[33] a Fab D1.3 antilysozyme,[34] and an immunoglobulin Kol2fb4[35] were obtained from the Brookhaven Protein Data Bank.[36] All calculations, i.e., sequence alignment (Figure 1), coordinate assignment, loop generation, MD, and EM, were performed on a Silicon Graphics workstation using Biosym software (Biosym Technologies).[29,37] Sequence

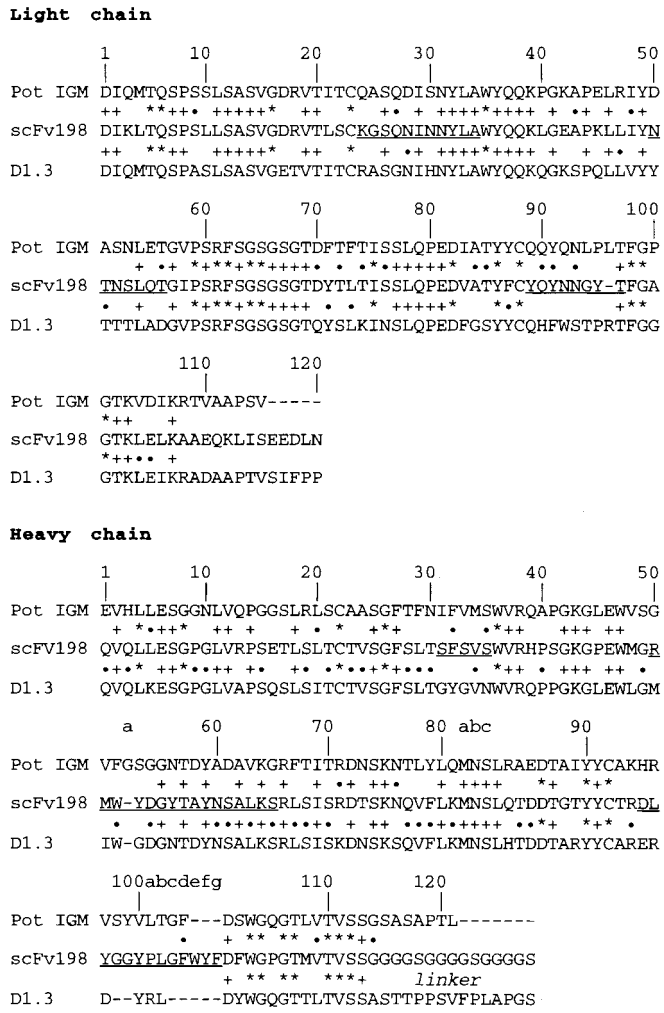

FIGURE 1 Sequence alignment of scFv198 with Pot IgM and D1.3. Residues numbers are designated according to Kabat[10]: (+), residues conserved in all three compared sequences; (●), residues conserved in scFv198 and one of the reference sequences; (★), residues conserved in 95% of known antibody sequences. CDR sequences are underlined.

alignment, loop generation, and coordinate assignment are integral routines of the HOMOLOGY module. Documented alignment was performed using Schuler's method[38] in manual and automatic mode. Resulting values correspond to denoted pairs of sequences or subsequences. For homology scoring, the evolutive PAM-250 protein alignment matrix was applied.[39] De novo loop generation was performed using the GENERATE_LOOP routine implemented in the HOMOLOGY module. The routine was modified by a Biosym macro command in order to produce a set of several hundreds of conformations. Van der Waals overlap penalty during the search was set to 0.6 Å. During the construction phase, EM calculations were performed to relieve accidental atomic overlaps. In the case of de novo constructed loops, energy terms of minimized structures were used for the evaluation of calculated conformations. Stereochemical quality of protein structure was investigated using the program PROCHECK.[30]

Docking

Docking was performed using the FIXED_DOCKING routine that is implemented in the DOCKING module. A docking grid with a resolution of 0.8 Å including Coulomb and van der Waals terms was created. The docking routine sampled statistical complex arrangements by repeated EM (set to a maximum of 200 steps) of a peptide and antibody assembly. After each minimization, the peptide was forced to adopt a new, randomly chosen starting orientation within the binding site. The maximal difference between the new starting position and the initial starting position was set to values of 3 Å (transposition) and 180° (rotation). During the docking procedure, the antibody frame was fixed, whereas all CDRs (complementarity-determining regions) were allowed to move. The peptide conformation was retained by restraint force constants of 5–10 kcal mol^{-1} $Å^{-2}$ of a flat-bottomed potential applied to 10 backbone restraints

and 10 side-chain restraints that were derived from nmr data. A set of 360 complex structures was generated. Complexes were analyzed with regard to energy terms, intramolecular and intermolecular interactions, buried surface area, side-chain exposure to the solvent, and stereochemical quality. The final complex was submitted to a MD calculation of 750 ps, applying the same restraints as in docking calculations. The complex structure was minimized and saved every 75 ps. The trajectories of the run were analyzed as described above. The selected complex was further submitted to a minimization of 200 iterations and a final minimization of 100 steps using no restraints in order to relax the system. Solvent- accessible surface was assessed by use of the program PROSTAT in the HOMOLOGY module. The probe radius was set to 1.4 Å. The buried surface was defined by contacting atoms at the complex interfaces. Residue and segment mobility was taken from the output of the MEANSQDISP routine of the ANALYSIS module.

RESULTS AND DISCUSSION

Peptide Structure

The complex between the scFv198 antibody fragment and the [G^{70}, Nle^{76}]MIR decapeptide antigen was investigated by means of 2D-TOCSY and 2D-TR-NOESY experiments (Figure 2). The spectroscopic investigations yielded 17 backbone–backbone, 36 backbone–side-chain, and 20 side-chain–side-chain distance constraints for the peptide conformation (Table I). A set of 150 spatial structures was generated by use of DG and simulated annealing calculations. This set of starting structures was submitted to 30 ps of MD calculations at 300 K. The nmr-derived interproton distances were applied as distance constraints at a level of 4 kcal mol^{-1} $Å^{-2}$. There was no substantial change in the peptide structure during the last 25 ps simulations, and this interval served to further analysis and conformational averaging (Table II). The observed peptide structure is characterized by a tight β-turn-like N-terminal loop and a C-terminus bent. This conformation is in good agreement with the nmr data (Figure 3) and similar type β-turns are commonly observed in antibody–peptide complexes.[13] It has also been shown that the [Ala^{76}]MIR decapeptide adopts a βIII-turn probably in solution.[5] Residue P^{69}, in position $i + 1$, induces the β-turn in the peptide backbone. The peptide conformation shows an alignment of the two bulky W^{67}, Y^{72}, and the linear Nle^{76} side-chains, which point toward the same general direction relative to the principle axis of the peptide backbone (Figure 4). It is very probable that this alignment is induced by the shape of the antibody binding channel, which forces the peptide backbone to adopt a more tight turn compared to the free state. Consequently, residue G^{70}

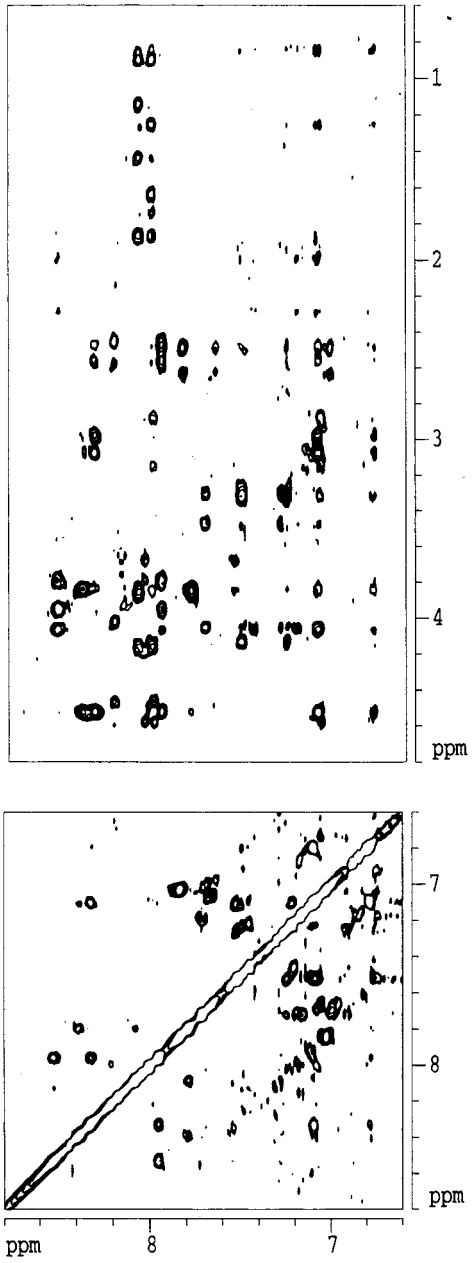

FIGURE 2 CH—NH (up) and NH—NH (down) regions of the TR-NOESY spectra of the [G^{70},Nle^{76}]MIR decapeptide in the presence of 2% mAb198 antibody in H_2O/D_2O, 95/5 v/v (pH 7.2, T = 4°C, mixing time = 200 ms). The water signal is suppressed with the WATERGATE sequence using field gradient pulses.

moves from the βIII-region to a more unusual region on the Ramachandran plot. The ease of structural adaptation of the peptide, due to the flexibility of residue G^{70}, should contribute to the high affinity binding of the [G^{70}, Nle^{76}]MIR derivative. Apart from the N-terminal turn, the conformation of the complexed peptide is stabilized by four additional internal hydrogen bonds, forming an

Table I Comparison Between (1) the NOE-Derived Interproton Distances (r_{NMR} in Å) of the Complexed [G^{70}, Nle^{76}]MIR Peptide, (2) the Corresponding Values in the Time-Averaged Structures from the Last 50 ps Period of the Restrained MD Simulation (r_{MD} in Å), and (3) the Minimized Structure after Docking (r_C in Å)

Protons		r_{NMR}	r_{MD}	r_C	Protons		r_{NMR}	r_{MD}	r_C
				Backbone–backbone					
N^{68}—$C^{\alpha}H$	N^{68}—NH	2.7–3.3	3.0	3.0	G^{73}—NH	G^{74}—NH	2.6–3.2	2.6	2.8
P^{69}—$C^{\alpha}H$	G^{70}—NH	2.2–2.8	2.1	2.2	G^{73}—$C^{\alpha}H$	G^{74}—NH	2.0–3.0[a]	2.4	2.5
G^{70}—$C^{\alpha}H$	G^{70}—NH	2.4–3.0	2.6	2.8	G^{73}—$C^{\alpha}H$	I^{75}—NH	3.8–4.4	4.5	4.7
G^{70}—NH	D^{71}—NH	2.7–3.3	3.2	3.3	G^{74}—$C^{\alpha}H$	G^{74}—NH	2.2–2.8	2.6	2.6
G^{70}—$C^{\alpha}H$	D^{71}—NH	2.7–3.3	3.1	2.5	G^{74}—NH	I^{75}—NH	2.9–3.5	3.2	3.1
D^{71}—$C^{\alpha}H$	D^{71}—NH	2.3–2.9	3.0	2.9	G^{74}—$C^{\alpha}H$	I^{75}—NH	2.4–3.0	3.1	2.8
D^{71}—NH	Y^{72}—NH	2.6–3.2	2.9	2.7	I^{75}—$C^{\alpha}H$	I^{75}—NH	2.4–3.0	3.0	2.9
D^{71}—$C^{\alpha}H$	Y^{72}—NH	3.0–4.0[a]	3.2	3.6	I^{75}—NH	Nle^{76}—NH	2.2–2.8	2.3	2.2
Y^{72}—$C^{\alpha}H$	Y^{72}—NH	1.9–2.5	2.5	3.0	I^{75}—$C^{\alpha}H$	Nle^{76}—NH	3.0–4.0[a]	3.6	3.6
Y^{72}—$C^{\alpha}H$	G^{73}—NH	2.2–2.8	2.6	2.3	Nle^{76}—$C^{\alpha}H$	Nle^{76}—NH	2.7–3.3[a]	3.1	3.0
G^{73}—$C^{\alpha}H$	G^{73}—NH	2.3–2.9	2.6	2.4					
				Backbone–side chain					
W^{67}—$C^{\alpha}H$	Y^{72}—$C^{\delta}H$	2.2–3.2	3.0	5.8	Y^{72}—$C^{\alpha}H$	Y^{72}—$C^{\beta 2}H$	2.6–3.6	3.5	3.0
W^{67}—$C^{\alpha}H$	Y^{72}—$C^{\varepsilon}H$	3.1–4.1	3.0	4.0	Y^{72}—$C^{\alpha}H$	Y^{72}—$C^{\delta}H$	2.3–3.3	2.2	2.4
P^{69}—$C^{\alpha}H$	P^{69}—$C^{\beta 1}H$	2.1–3.1	2.3	2.1	G^{73}—NH	Y^{72}—$C^{\beta}H$	3.4–4.4	4.5	5.0
P^{69}—$C^{\alpha}H$	P^{69}—$C^{\beta 2}H$	2.3–3.3	2.8	2.8	G^{73}—NH	Y^{72}—$C^{\delta}H$	3.5–4.5	4.5	4.0
P^{69}—$C^{\alpha}H$	P^{69}—$C^{\gamma}H$	2.2–3.2	3.9	3.4	G^{73}—$C^{\alpha}H$	Y^{72}—$C^{\varepsilon}H$	4.5–5.5	4.6	4.6
P^{69}—$C^{\alpha}H$	Y^{72}—$C^{\delta}H$	3.5–4.5	3.9	4.0	I^{75}—NH	I^{75}—$C^{\beta}H$	2.3–3.3	4.0	3.9
G^{70}—NH	P^{69}—$C^{\beta 1}H$	3.2–4.2	4.0	4.0	I^{75}—NH	I^{75}—$C^{\gamma 11}H$	2.7–3.7	3.2	3.0
G^{70}—NH	P^{69}—$C^{\beta 2}H$	3.3–4.3	4.2	4.0	I^{75}—NH	I^{75}—$C^{\gamma 12}H$	2.5–3.5	3.2	3.1
G^{70}—NH	P^{69}—$C^{\gamma}H$	4.2–5.2	5.1	5.4	I^{75}—NH	I^{75}—$C^{\gamma 2}H$	2.9–3.9	3.3	3.7
G^{70}—$C^{\alpha}H$	G^{70}—$C^{\alpha 2}H$	1.7–2.7	1.8	1.7	I^{75}—$C^{\alpha}H$	I^{75}—$C^{\beta}H$	2.4–3.4	2.3	2.4
D^{71}—NH	D^{71}—$C^{\beta 1}H$	2.0–3.0	3.2	2.8	I^{75}—$C^{\alpha}H$	I^{75}—$C^{\gamma 11}H$	2.9–3.9	3.8	3.8
D^{71}—NH	D^{71}—$C^{\beta 2}H$	2.2–3.2	3.8	3.8	I^{75}—$C^{\alpha}H$	I^{75}—$C^{\gamma 2}H$	2.0–3.0	2.5	2.5
D^{71}—NH	Y^{72}—$C^{\delta}H$	4.0–4.5	4.3	5.9	Nle^{76}—NH	I^{75}—$C^{\beta}H$	2.7–3.7	3.6	3.7
Y^{72}—NH	D^{71}—$C^{\beta}H$	2.7–3.7	3.6	5.9	Nle^{76}—NH	I^{75}—$C^{\gamma}H$	2.0–3.0	2.6	2.1
Y^{72}—$C^{\alpha}H$	D^{71}—$C^{\beta}H$	4.1–5.1	5.0	3.9	Nle^{76}—NH	Nle^{76}—$C^{\beta 1}H$	2.4–3.4	3.4	3.5
Y^{72}—NH	Y^{72}—$C^{\beta}H$	2.1–3.1	2.6	2.7	Nle^{76}—NH	Nle^{76}—$C^{\beta 2}H$	3.2–4.2	4.0	4.0
Y^{72}—NH	Y^{72}—$C^{\delta}H$	2.9–3.9	3.9	3.9	Nle^{76}—NH	Nle^{76}—$C^{\gamma}H$	2.3–3.3	2.9	2.9
Y^{72}—$C^{\alpha}H$	Y^{72}—$C^{\beta 1}H$	2.8–3.8	2.6	2.5	Nle^{76}—$C^{\alpha}H$	Nle^{76}—$C^{\gamma}H$	3.0–4.0	3.8	4.0
				Side chain–side chain					
N^{68}—$C^{\beta 1}H$	N^{68}—$C^{\delta 1}H$	2.2–3.2	2.2	2.1	Y^{72}—$C^{\delta}H$	Y^{72}—$C^{\varepsilon}H$	1.8–2.8	2.5	2.4
N^{68}—$C^{\beta 2}H$	N^{68}—$C^{\delta 1}H$	2.8–3.8	3.6	2.9	Y^{72}—$C^{\delta}H$	I^{75}—$C^{\delta}H$	4.2–5.2	4.4	4.8
N^{68}—$C^{\beta 1}H$	N^{68}—$C^{\delta 2}H$	2.8–3.8	3.3	3.5	Y^{72}—$C^{\delta}H$	Nle^{76}—$C^{\gamma}H$	3.6–4.6	4.3	3.7
N^{68}—$C^{\beta 2}H$	N^{68}—$C^{\delta 2}H$	3.2–4.2	3.9	3.7	Y^{72}—$C^{\varepsilon}H$	I^{75}—$C^{\delta}H$	3.9–4.9	4.5	4.1
N^{68}—$C^{\delta 1}H$	N^{68}—$C^{\delta 2}H$	1.7–2.7	1.9	1.7	Y^{72}—$C^{\varepsilon}H$	Nle^{76}—$C^{\gamma}H$	4.1–5.1	4.3	4.5
D^{71}—$C^{\beta 1}H$	D^{71}—$C^{\beta 2}H$	1.7–2.7	1.8	1.7	I^{75}—$C^{\beta}H$	I^{75}—$C^{\gamma 1}H$	2.1–3.1	2.5	2.5
D^{71}—$C^{\beta}H$	Y^{72}—$C^{\delta}H$	3.4–4.4	4.4	5.8	I^{75}—$C^{\delta}H$	I^{75}—$C^{\gamma 1}H$	2.5–3.5	2.5	2.5
Y^{72}—$C^{\beta 1}H$	Y^{72}—$C^{\beta 2}H$	1.7–2.7	1.7	1.7	I^{75}—$C^{\gamma 1}H$	I^{75}—$C^{\gamma 2}H$	2.1–3.1	2.8	2.5
Y^{72}—$C^{\beta 1}H$	Y^{72}—$C^{\delta}H$	2.3–3.3	2.6	2.3	I^{75}—$C^{\delta}H$	Nle^{76}—$C^{\beta}H$	4.3–5.3	4.9	4.9
Y^{72}—$C^{\beta 2}H$	Y^{72}—$C^{\delta}H$	2.8–3.8	2.7	3.1	I^{75}—$C^{\gamma}H$	Nle^{76}—$C^{\gamma}H$	2.9–3.9	3.1	2.4

[a] Exact distances are not accessible because of peak overlap.

intramolecular network around the central β-turn-like motif. In conclusion, it can be stated that the [G^{70}, Nle^{76}]MIR peptide is a prestructured ligand in solution showing a characteristic N-terminal β-turn. Binding to the antibody presumably forces the hydrophobic residues W^{67}, Y^{72}, and Nle^{76} to an aligned position, whereas the β-turn is slightly deformed allowing then residues W^{67}, N^{68}, and D^{71} to form numerous contacts.

Construction of the scFv198 Framework

Among the known structures of antibody fragments, those of human Pot IgM[33] and anti-lysozyme D1.3[34]

Table II Dihedral Angles of [G^{70}, Nle^{76}]MIR Assessed by Means of DG and MD Calculations

Residue	ϕ	ψ	ω	χ^1	χ^2	χ^3	χ^4
W^{67}		−63.6	174.8	−68.3	−65.2		
N^{68}	−78.8	166.4	174.3	−70.0	−66.7		
P^{69}	−68.6	103.8	−170.0	26.3	−35.2	29.1	
G^{70}	146.7	−71.2	169.5				
D^{71}	−61.3	−49.2	165.8	50.9	138.6		
Y^{72}	−94.2	71.6	−174.4	−79.1	174.8	−177.5	−1.6
G^{73}	−109.8	−62.1	174.4				
G^{74}	−107.3	41.3	179.7				
I^{75}	−131.3	−53.6	−179.4	69.0	149.5		
Nle^{76}	−137.6	67.2	164.9	−169.7			

show the highest score of homology with scFv198 (Figure 1). Thus, their respective sequences and structures were used as templates for the model construction. Global comparison of sequences yielded homology scores of 51–72% for the heavy chains and 56–65% for the light chains. Comparison of CDR sequences revealed canonical properties for CDRs L1, L2, H1, and H2 (Figure 1), thus allowing the construction of these loops according to the homology procedure. Atomic coordinates of CDRs L1 and L2 were derived from those of Pot IgM, whereas those of CDRs H1 and H2 were the coordinates of D1.3. After coordinate assignment, each CDR was submitted to several stages of energy minimization. Conformational analysis confirmed a positional conservation of all polar residues Asx or Glx, as well as aromatic residues. Moreover, at conservative mutation sites the overall side chain orientation of residues was retained in comparison to the corresponding template molecule (Figure 5).

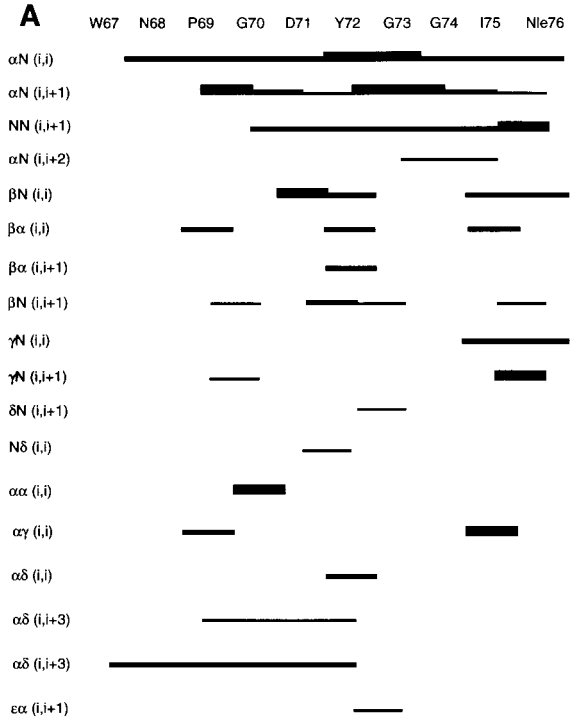

FIGURE 3 Summary of the ^1H /^1H TR-NOE connectivities of the [G^{70},Nle^{76}]MIR decapeptide in the presence of 2% mAb198 antibody in H_2O/D_2O, 95/5 v/v solution. The TR-NOE intensities are represented by different line thicknesses and they are classified as strong, medium, or weak.

The CDR-L3 has no resemblance with any of the resolved antibody fragments in databases. In fact, due to the absence of the *cis*-P95 key residue replaced by Y95, present in most of other antibodies and the deletion of the L96 residue (Figure 1), the L3 loop was considered as noncanonical and was constructed de novo. For conformational sampling, a set of about 1000 loop structures was generated, 200 of which were acceptable to be attached to the anchor points. All these fitting loops were submitted to 500 steps of steepest descent EM and 700 steps of conjugate gradient EM keeping the framework tethered. Terms of nonbound energies were evaluated using a cutoff distance of 12 Å. Thereafter, two loop conformations that exhibited lowest energy were initiated for a 60 ps MD run at 300 K. The resulting conformations revealed very close backbone conformations and side-chain locations to each other. The loop exhibiting the best overlap of nonmutated residues with those of Pot IgM was chosen. Again, the whole framework was subjected to EM. The final conformation is equivalent to that of the Pot IgM CDR-L3 except residues *cis*-P95 and L96 (Figure 5).

A critical part in the construction scheme of scFv198 was the 13 residue loop CDR-H3. It is much longer than the equivalent CDRs of Pot IgM (9 residues) and D1.3 (6 residues). Moreover, low homology scores impaired the use of homology procedures. On the other hand, a de novo generation of a 13-residue

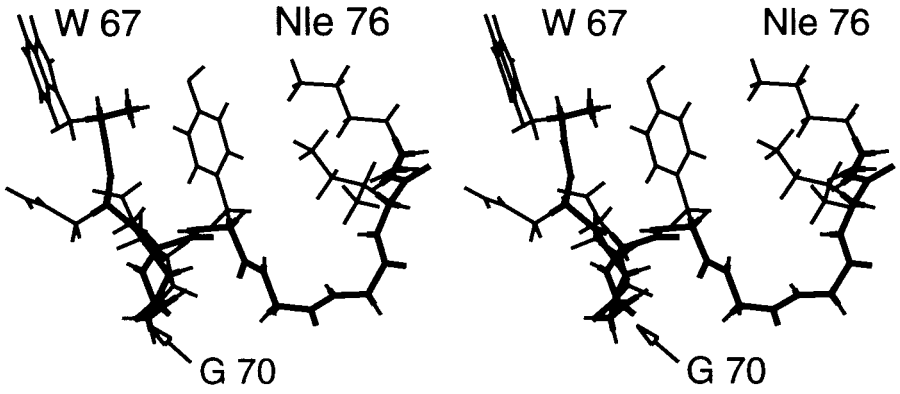

FIGURE 4 Stereoviews of the time-averaged structure of the [G^{70},Nle^{76}]MIR decapeptide. The structure was generated by means of restrained MD simulations.

fragment required considerable structural information to yield a reliable conformation. Therefore, a third reference structure was needed for the construction of that segment. The 15-residue CDR-H3 of Kol2fb4[35] was chosen to serve as a template. Obviously, the sequence homology score is relatively low between the two H3 loops (31%) but it is still within the limits of modeling techniques. Atomic coordinates of CDR-H3 of Kol2fb4 were transferred to the CDR sequence of scFv198. Naturally, the deletion of the two residues, S100e and C100f, disrupted the initial angle distribution of neighboring residues. The deviations from standard parameters were corrected by optimization and the stereochemical quality of the structurated sequence was investigated using PROCHECK. The completed CDR loop was connected to the antibody fragment. An EM calculation was run including the whole backbone of scFv198, modeled so as eliminating accidental atomic overlaps. Noteworthy, the resulting loop geometry resembled the template loop of Kol2fb4, especially in the functionally important turn region (Figure 5). The final structure appeared to be consistent within a resolution of 2 Å, thus exhibiting a high stereochemical quality (Figure 6).

Docking

Calculational docking of proteins includes different issues such as location of the binding site, packing of

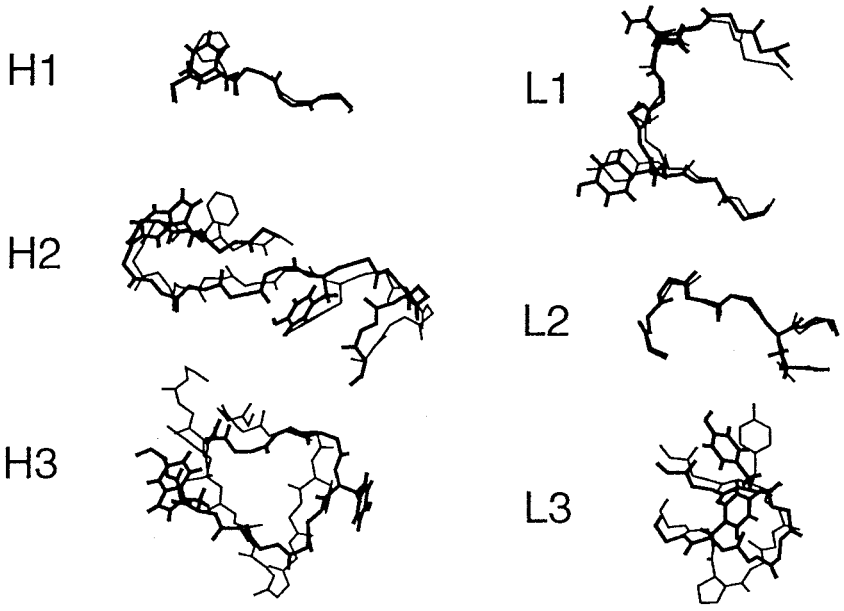

FIGURE 5 The predicted conformation (heavy lines) for each CDR of scFv198 is shown superimposed on the respective conformations of the crystal structure (thin lines) of Pot IgM (loops H1, H2, L1, L2, and L3) and of Kol2fb4 (loop H3).

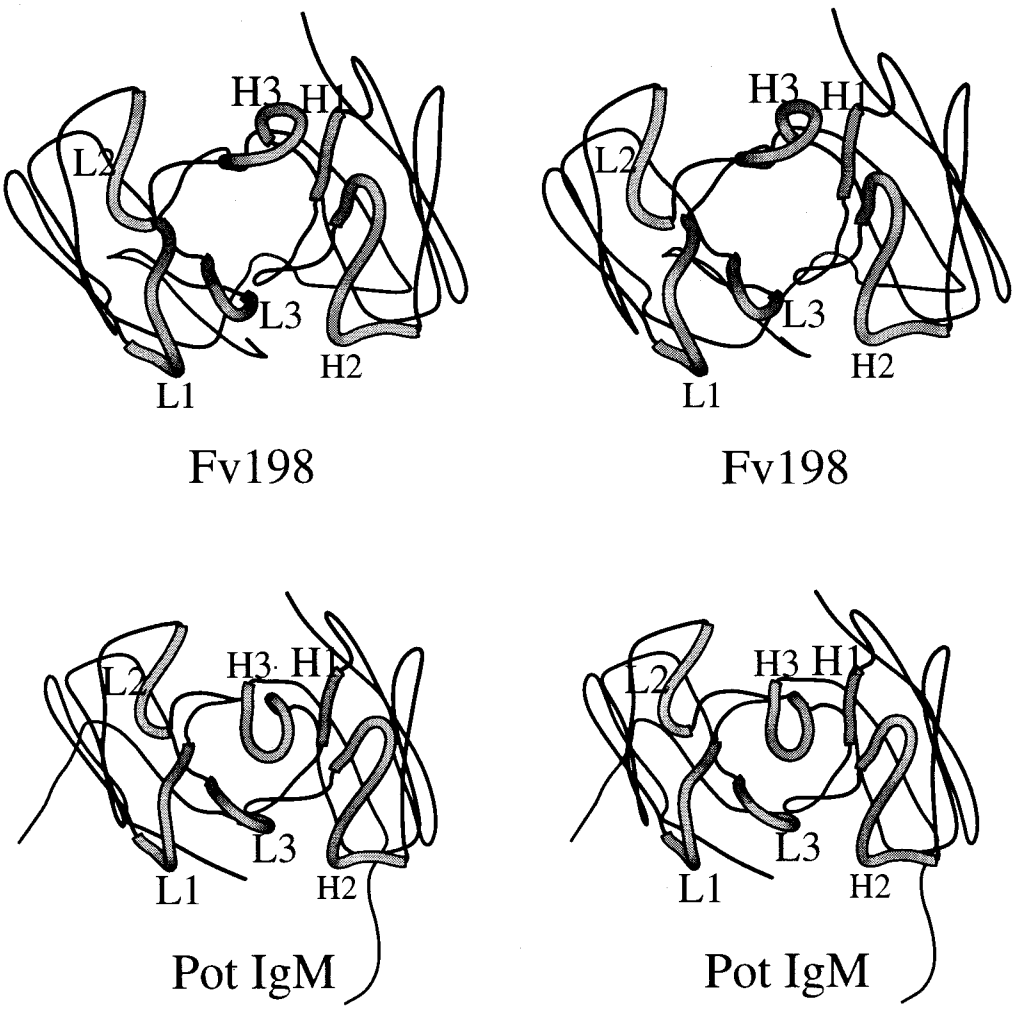

FIGURE 6 Compared "top" stereoview (MOLSCRIPT[56]) representation of all CDRs (thick ribbons) in the context of the light and heavy chain variable domains for the scFv198 (up) and Pot IgM (down) antibodies. The light chain is situated on the left side.

irregular objects, and evaluation of surface complementarity. However, criteria for protein association have been defined[40,41] and several docking routines have been described.[42–47] It was shown that prediction of binding site structures yielded correct results when "directed modeling" was applied.[16] The scFv198 binding site is formed by a channel with a hydrophobic pocket at each end and a positive charged H2 R50 residue at the center of the bottom. The channel walls are more hydrophilic, thus presenting potential locations for hydrogen bonds to the peptide ligand. For docking calculations, the ligand was placed near this putative binding site. The docking routine generated randomized ligand–antibody assemblies using a MC algorithm. These assemblies were submitted to EM calculations employing full molecular representation of the peptide antigen and the antibody binding site.

Antibody CDRs and peptide side-chains were not constrained in mobility. This allowed sampling of the conformational space toward "induced fit" shapes. Approximations were introduced into the docking routine by defining peptide backbone restraints and by fixing the antibody framework. Without application of backbone restraints, the peptide was progressively deformed by strong local interactions in the course of the 200 simulated docking reactions per run. Therefore, 10 backbone restraints and 10 side-chain restraints were applied during the docking calculation. The problem of multiple energy minima was overcome by extensive conformational sampling. The total energy of the assembly or complex, respectively, was used as a transformation index, along the reaction coordinate of the simulated binding reaction. The advantage of EM-based docking is that the relative total energy is accessible, through simulations, along

with related structural details of the complex. That a few low-energy structures were frequently found supported our confidence in the results.

The different binding geometries, routinely observed, covered a scale from plausible to rather implausible complexes, with respect to their steric arrangements and the spectrum of interactions. This finding was partially due to the fact that docking calculations were performed in the absence of solvent molecules and therefore energy contributions of the burial of hydrophobic side chains in the binding site was presumably underestimated. However, each of the most frequently found complex geometries reflected a plausible conformation and the one finally chosen had a frequency of 38%. Evaluation of the observed complexes invoked comparison of relative total energies, whereby special attention was paid to the contributions of the applied restraints. A small set of 20 constraints of the total of 73 nmr restraints was used for the docking simulation and the final conformation was in accordance with all but four nmr constraints: W^{67}—CαH–Y^{72}—CδH, D^{71}—NH–Y^{72}—CδH, Y^{72}—NH–C^{71}—CβH, and D^{71}—CβH–Y^{72}—CδH (Table I). These violations are local imperfections, but considering the precision of the approach these distances are well within the resolution of the model. Fixing of the antibody framework excluded its contributions to energy terms, which in turn led to relatively larger weighting of interactions to the energy terms.

The final complex was submitted to 750 ps of MD simulation at 300 K. Constraints were also applied, limiting the peptide conformation to the geometry derived from nmr investigations. The MD simulation led to minor changes in the global arrangement, though the number of atom contacts and hydrogen bonds increased. This effect was mostly attributed to side-chain reorientation and small backbone displacements. The overall structure showed physicochemical surface complementarity and was stereochemically plausible.

Antibody–Antigen Interactions

Contacts and Bonds. The complex between [G^{70}, Nle^{76}]MIR and scFv198 is stabilized by 12 intermolecular hydrogen bonds, two central ionic interactions, and 38 van der Waals contacts (Table III). The W^{67}, Y^{72}, and I^{75} side chains of the MIR peptide form a saddle-shaped surface, in which, the W^{67} and I^{75} peptide residues, at the lower points, occupy two hydrophobic pockets in the binding site. The only peptide residues without any contact with the antibody are P^{69} and G^{73}. Seven nonaromatic and nine aromatic residues of the antibody contact the peptide antigen. The antibody residues making a major contribution to binding are situated on CDRs L3, H2, and H3, and one residue from the framework is involved. The important N-terminal turn of the peptide is flanked largely by CDR loop L3 on one side and loop H2 on the other. Loop L3 significantly contributes to binding with the formation of 3 hydrogen bonds and 16 van der Waals contacts to the antigen (Table III). The backbone of L3 interacts mainly with the W^{67} and Y^{72} side chains of the peptide, whereas the L3 Y97 side chain contacts the peptide backbone (Figure 7). The W52, Y56 and A58 side chains of loop H2 form numerous C—C contacts with the peptide. Two additional hydrogen bonds are observed between W^{67}—N$^{\epsilon}$H and D^{71}—CO of [G^{70}, Nle^{76}]MIR and H2 S61—O$^{\gamma}$H and L3 Y97—O$^{\eta}$H of the antibody, respectively. A major stabilization derives from the presence of the H2 R50 and H2 K64 residues on the bottom of the antibody binding site, which form three hydrogen bonds with the peptide ligand. In particular, the guanidinium group of R50 fixes the peptide backbone by establishing two hydrogen bonds with the G^{70}—CO group of the antigenic peptide. In addition, long-distance Coulomb forces are generated between the negatively charged D^{71} side chain of the peptide on one hand and the H2 R50 (10.2 Å) and H2 K64 (6.3 Å) antibody side chain on the other hand. It deserves to be noted that charged residues close to the binding site are likely to be important in electrostatic steering, as has been demonstrated by Kozack and Subramaniam.[48]

Surface Properties. Surface complementarity forms the basis of antibody–ligand binding (Table IV). In the case of charged ligands the key forces determining antibody specificity are electrostatic interactions. On the other hand, more hydrophobic ligands rely on the burial of nonpolar side chains in hydrophobic pockets and the formation of numerous contacts. Both processes are generally accompanied by the formation of a specific pattern of hydrogen bonds, depending on the polarity of ligand side chains and backbone orientation within the binding cleft. The [G^{70}, Nle^{76}]MIR peptide contains charged groups (N-terminus, D^{71} side chain and C-terminus) as well as hydrophobic side chains (W^{67}, Y^{72}, Ile^{75}, Nle^{76}). As expected, the binding channel of the scFv198 model reflects the distribution of charges and the hydrophobicity of its cognate peptide ligand. The transfer of the hydrophobic surfaces of interaction from a solvated to a complexed environment is accompanied by change in free energy. Thus, the change of solvent-accessible surface (SAS) may serve as a measure of binding

Table III Hydrogen Bonds and Intermolecular Contacts in the [G^{70}, Nle^{76}]MIR-Fv198 Complex

Intermolecular Hydrogen Bonds

[G^{70}, Nle^{76}] MIR	Fv198	Distance (Å)	Angle (°)
W^{67}—NH_3^+	L3 N93—CO	2.2	134
W^{67}—N^{ε}	H2 S61—O^{γ}H	1.9	171
W^{67}—N^{ε}	H2 S61—O^{γ}	2.9	NA
N^{68}—$C^{\gamma}O$	H2 Y59—NH	2.2	151
N^{68}—N^{δ}H	H2 K64—N^{ε}	2.4	158
G^{70}—CO	H2 R50—N^{ε}H	2.4	143
G^{70}—CO	H2 R50—N^{η}H	1.8	170
D^{71}—CO	L3 Y95—O^{η}H	1.9	142
Y^{72}—O^{η}H	L3 N92—CO	1.7	176
G^{74}—CO	H3 G100c—NH	2.3	134
G^{74}—CO	H3 F100d—NH	2.1	171
I^{75}—CO	L1 Y32—O^{η}H	1.8	163

Van der Waals Contacts[a]

Peptide	Antibody	Peptide	Antibody
W^{67}—N	H2 K64—N^{η}	D^{71}—CO	L3 Y95—O^{η}
W^{67}—N	H2 Y59—CO	Y^{72}—O^{η}	L3 N93—CO
W^{67}—C^{β}	H2 S61—O^{γ}	G^{73}—C^{α}	H2 W52—$C^{\eta 2}$
W^{67}—$C^{\delta 2}$	H2 S61—O^{γ}	G^{73}—C^{α}	H2 W52—$C^{\zeta 2}$
W^{67}—$C^{\varepsilon 3}$	H2 S61—O^{γ}	G^{73}—C	H2 W52—$C^{\eta 2}$
W^{67}—C^{ζ}	L3 N93—CO	G^{73}—C	H2 W52—$C^{\zeta 2}$
W^{67}—$C^{\zeta 3}$	L3 N93—CO	G^{74}—C^{α}	H3 P100a—CO
W^{67}—$C^{\eta 2}$	L3 N93—C	G^{74}—C^{α}	H3 F100d—$C^{\delta 1}$
W^{67}—$C^{\eta 2}$	L3 N93—CO	I^{75}—C	L1 Y32—O^{η}
W^{67}—$C^{\zeta 3}$	L3 G94—C^{α}	I^{75}—CO	L1 Y32—O^{η}
N^{68}—C^{β}	H2 Y56—$C^{\varepsilon 1}$	I^{75}—C^{α}	L1 Y32—O^{η}
N^{68}—C^{β}	H2 A58—C^{β}	I^{75}—C^{β}	L1 Y32—C^{ζ}
N^{68}—C^{γ}	H2 Y56—$C^{\varepsilon 1}$	I^{75}—C^{β}	L1 Y32—$C^{\varepsilon 2}$
G^{70}—C	H2 A58—C^{β}	I^{75}—$C^{\gamma 2}$	L3 Y91—$C^{\delta 2}$
D^{71}—C^{α}	L3 Y95—C^{ζ}	I^{75}—$C^{\gamma 2}$	H3 Y100f—O^{ζ}
D^{71}—C^{β}	FW[b] W47—$C^{\eta 2}$	I^{75}—$C^{\delta 1}$	L3 Y91—C
D^{71}—C^{β}	L3 Y95—Φ[c]	I^{75}—$C^{\delta 1}$	L3 Y91—CO
D^{71}—C	L3 Y95—$C^{\varepsilon 1}$	I^{75}—$C^{\varepsilon 1}$	L3 Y95—$C^{\varepsilon 1}$
D^{71}—C	L3 Y95—C^{ζ}	Nle^{76}—C^{ε}	L3 N92—CO

[a] Intermolecular atom pair contacts were defined by distances (Å) equal or less than C—C, 4.0; C—N, 3.7; C—O 3.6; N—N, 3.3; N—O, 3.3; O—O, 3.2.

[b] FW denotes antibody framework.

[c] Φ denotes a central position with respect to the aromatic ring leading to contacts with all carbon atoms.

strength.[49] An approximate value for the energy difference is 24 cal per $Å^2$ of buried surface.[50] The buried surface area in the examined complex model is calculated as 1051 $Å^2$ equivalent to a gain of 25 kcal mol^{-1} of free energy. Another estimation is given by the formula $\Delta C_p = -119 + 0.20\ (\Delta SAS)$,[51] which leads to 24 kcal mol^{-1} at 298 K. The buried surface area of the MIR peptide (516 $Å^2$) is similar to that of the antibody (535 $Å^2$). It has been also reported that the change of SAS in protein–antibody complexes is about 1500 $Å^2$ (in each complex)[52] whereas peptide–antibody complexes show smaller changes. The hydrophilic/hydrophobic ratio of the buried surface does not differ from the average ratio for the two molecules, indicating that no particular hydrophobic or hydrophilic surface patches are in contact.

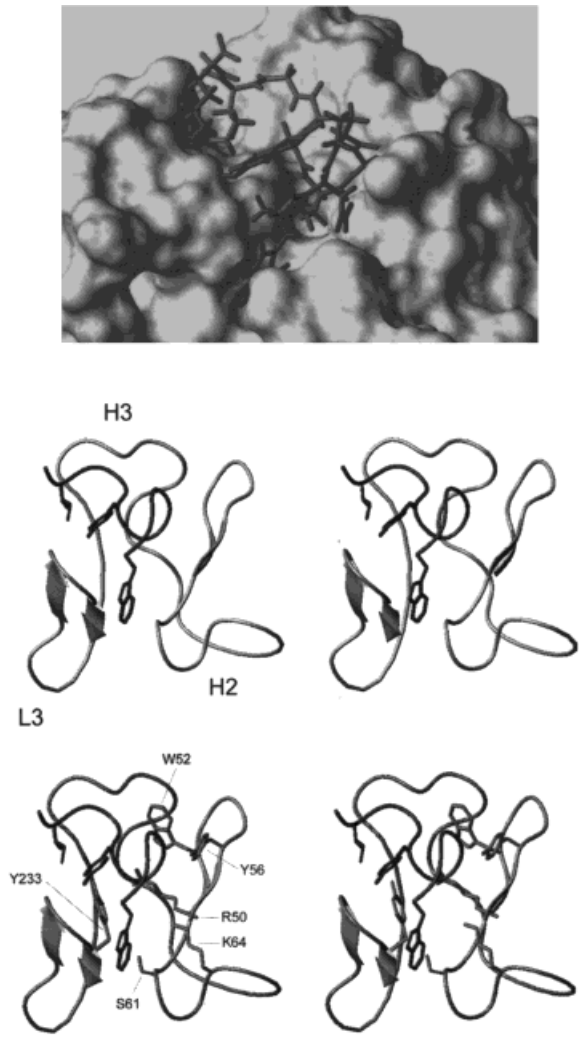

FIGURE 7 Complex between the [G^{70}, Nle^{76}]MIR decapeptide and scFv198. The antibody binding site forms a channel. The inner surface is dominated by aromatic side chains of tyrosine and tryptophan. The displayed potential surface is composed of Coulomb and van der Waals contributions. Bulky and hydrophobic side chains of the decapeptide are buried in the binding site (top). The backbones of CDR loops L3, H2 and H3 (middle) and their side chains in contact with the decapeptide (bottom) are shown.

Rearrangements and Mobility. Formation of the antigen–antibody complex consists either of side-chain movements, CDR rearrangements, and changes of the relative orientation of V_H and V_L,[13,40,53,54] or of significant conformational changes.[55] Dynamic simulation gives information about rearrangements accompanying the docking reaction as well as segmental flexibility in the complexed state. Taking into account the approximate nature of simulation, calculated conformational changes may be regarded as indicators for possible structural transitions.

In the course of docking calculations, only small changes in the CDR loop conformations were observed. Though the CDR sequences were not restrained, EM calculations mostly affected side-chain orientations and rms values of side-chain heavy atoms amounted to 0–0.4 Å. In contrast, the peptide backbone was restrained during the docking process. Nevertheless, a rotation of about 90° between both the N-terminal loop and the C-terminus occurred, which especially involves the ϕ/ψ angles of G^{73}. This finding is reflected by small rms values of 0.5 and 0.7 Å for the segment backbones, and by a large value (3.3 Å) for the whole peptide backbone. It is important to note that this rotation enables the W^{67}, Y^{72}, and Ile^{75} peptide side chains to enter the binding site simultaneously.

The complex was subjected to a restrained MD simulation of 750 ps at 300 K. Given the trajectories of CDR loops and the peptide from the dynamic simulation, potential relative mobilities were assessed in terms of self-diffusion parameters. Therefore, we determined the mean square amplitudes of CDR sequences and peptide residues and the observed mobilities of CDRs in the complexed state were in the range from 0.15 to 0.38 $Å^2$ with the exception of H3 CDR, which exhibits an exceptionally higher mobility (1.07 $Å^2$; Table IV). Reported values of $\langle x \rangle^2$ from x-ray studies are in the range of 0.1–0.4 $Å^2$ and mobilities are normally retained upon complexation.[16,40] Figure 8 highlights the markedly different mobilities within the contacting residues of the complex. Loops L3, H2, and H3 are exposed to the antigen and constitute nearly the whole binding surface of the antibody. However, the high mobility of the H3 loop stems from the lack of contacts with the framework, rather than from antigen contacts. Comparison of the percentage of buried surface and the relative mobility (Table IV) indicates the tendency of high mobility at exposed sites. The relative mobilities of the peptide antigen, which range from 0.61 to 3.50 $Å^2$, are higher than those of the antibody. The flat-bottomed potential of the applied restraints allowed a fairly free movement of the peptide within the defined interproton distance limits. However, the movements of the antigen and CDRs appear to be concerted so that distances at the interaction sites remained roughly constant.

CONCLUSION

The conformation of the complexed peptide antigen [G^{70}, Nle^{76}]MIR was derived by means of 2D-nmr and molecular modeling. Similar to other peptides of

Table IV Properties of scFv198 and [G^{70}, Nle^{76}]MIR

scFv198	L1	L2	L3	H1	H2	H3	FW[e]	Total
Total SAS[a] (Å^2)	619	406	308	103	1114	638	9480	12668
Polar SAS (Å^2)	358	205	144	3	454	139	4067	5370
Hydrophobic SAS (Å^2)	261	201	164	100	660	499	5413	7298
SAS fraction per residue (Å^2)	0.29	0.33	0.22	0.12	0.40	0.28	0.29	0.30
Total buried SAS (Å^2)	48	0	181	0	180	92	34	535
Polar buried SAS (Å^2)	22	0	87	0	86	49	0	244
Hydrophobic buried SAS (Å^2)	26	0	94	0	94	43	34	291
Percentage of buried SAS (%)	8	0	59	0	16	14	0.3	4
Mobility[b] (Å^2)	0.32	0.15	0.38	0.24	0.35	1.07	nd	
SD of mobility (Å^2)	0.07	0.03	0.09	0.04	0.05	0.45	nd	
No. of hydrogen bonds	1	0	3	0	6	2	0	12
No. of contacts[c]	5	0	16	0	13	3	1	38
Mean packing density[d]	1.00	1.00	0.96	0.84	1.05	1.01	1.02	1.01

[G^{70}, Nle^{76}]MIR	W^{67}	N^{68}	P^{69}	G^{70}	D^{71}	Y^{72}	G^{73}	G^{74}	I^{75}	Nle^{76}	Total
Total SAS[a] (Å^2)	272	95	145	65	87	105	68	82	140	221	1279
Polar SAS (Å^2)	70	75	25	25	37	44	35	39	38	79	466
Hydrophobic SAS (Å^2)	202	20	120	40	51	61	33	43	101	142	812
SAS fraction per residue (Å^2)	0.76	0.58	0.81	0.74	0.52	0.42	0.75	0.93	0.83	0.82	0.70
Total buried SAS (Å^2)	159	39	0	30	83	64	13	30	81	17	516
Polar buried SAS (Å^2)	31	22	0	13	40	22	13	22	13	0	174
Hydrophobic buried SAS (Å^2)	128	17	0	17	43	43	0	9	69	17	342
Perc. of buried SAS (%)	58	41	0	46	95	61	19	37	58	12	40
Mobility[b] (Å^2)	0.88	1.94	1.96	0.61	0.85	0.97	1.03	0.97	1.91	3.50	
SD of mobility (Å^2)	0.09	0.51	0.42	0.06	0.27	0.14	0.16	0.12	0.23	0.48	
No. of hydrogen bonds	3	2	0	2	1	1	0	2	1	0	12
No. of contacts[c]	10	3	0	1	6	1	4	2	10	1	38
Packing density[d]	0.92	0.90	1.11	0.97	0.92	1.37	0.96	0.96	0.98	0.98	1.02

[a] SAS values were determined using PROSTAT with a probe radius of 1.4 Å.
[b] Mobility is given as square amplitude of self-diffusion during 600 ps of MD.
[c] Intermolecular atom pair contacts were defined by distances (Å) equal or less than C—C, 4.0; C—N, 3.7; C—O, 3.6; N—N, 3.3; N—O, 3.3; O—O, 3.2.
[d] Packing density is calculated using the program QPACK. A value of 1 corresponds to ideal packing.
[e] FW denotes antibody framework.

the MIR family, the examined derivative adopts a type β-turn fold in the N-terminal region and an unusual ϕ/ψ angle combination at G^{70}. The complex structure revealed the antibody binding site as being the main inductor of this conformation. The peptide was docked to the antibody model of scFv198 that has been constructed beforehand. Extensive configurational sampling via a MC minimization routine yielded a favorable final complex structure with a high probability (38%). Analysis of the model complex in terms of surface complementarity showed many features commonly found in antibody–peptide complexes. The unusual steric properties of the [G^{70}, Nle^{76}]MIR peptide (three bulky residues) might have resulted in the antibody binding site having abnormal structural characteristics, which was not the case. It should be stressed that the antibody was targeted against the human AChR, but it binds the [G^{70}, Nle^{76}]MIR peptide with high affinity. In the complex structure presented here, all peptide residues except P^{69} are in contact with the antibody binding site and they probably correspond to the maximum length that can be accommodated in the binding groove.

Antigenic peptides are valuable tools for the investigation of immunocomplexes from autoimmune diseases. The conformation of the antibody-bound peptide antigen should, in the optimal case, reflect the conformation of the parent sequence in the protein. This relation is most probable when both structures, the natural epitope and the mimicking peptide, are equally recognized by an antibody. In the case of [G^{70}, Nle^{76}]MIR, the peptide has a high affinity for a

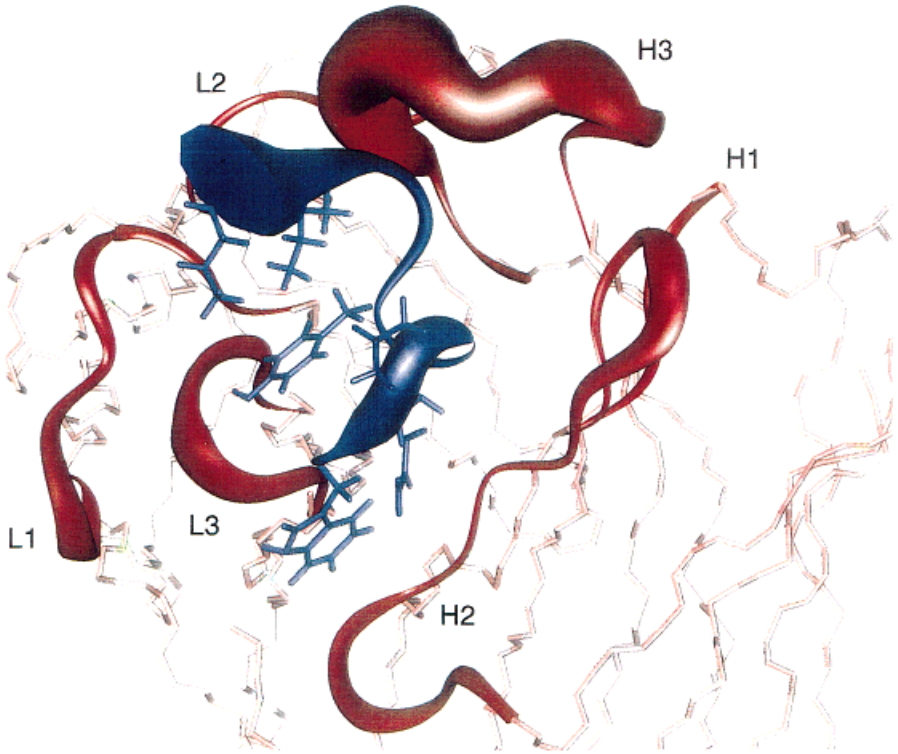

FIGURE 8 The flexibility of the peptide backbone of the antigenic decapeptide (blue) and the antibody CDRs (red-brown) in the scFv198–[G^{70},Nle^{76}]MIR complex are shown. The underlying data were derived from the last 50 ps of the MD simulation of the complex. The scale of the rendering is proportional to the mobility of the backbone.

monoclonal antibody raised against the MIR epitope of the protein. The applied technique of the "directed modeling" of the antibody structure consisted of a combination of knowledge-based homology modeling of the global geometry and "induced-fit" refinement of the local conformation by restrained dynamic simulation of the complex. The analysis of the complex structure gave insight into some structural and functional characteristics of an AChR-mimicking peptide as follows: (a) Four bulky residues (W^{67}, Y^{72}, I^{75}, and Nle^{76}) form numerous hydrophobic contacts with the antibody (Table III). (b) The N-terminal β-turn, which is imposed on the conformation by the presence of residue P^{69}, is an indispensable feature for the recognition process,[6–8] as it has also been shown for other MIR sequences.[5] This loop structure is required for the fitting of the bulky residues in the binding site of the antibody. (c) A negatively charged residue within the loop sequence (D^{71}) is exposed to the positively charged bottom of the binding site. The charge is supposed to affect the orientation of the ligand (electrostatic steering) and to stabilize the complex by the formation of hydrogen bonds and Coulomb interactions. This is in agreement with the fact that D^{71} has been found indispensable for antibody binding to the MIR peptide.[7,8] (d) Alignment of the peptide hydrophobic residues in the complexed state suggests a reorientation between the N-terminus and the C-terminus of the peptide via a rotation in the "linker" sequence G^{73}–G^{74} upon complexation.

It has been shown, in muscle cell culture experiments, that scFv198 is capable of shielding the MIR of the AChR and thus efficiently protecting the AChR against the destructive activity of the pathogenic autoantibodies from human patients.[24] We intend to investigate the applicability of this observation for the therapy of MG patients. This will require the enhancement of the affinity of scFv198, for MIR and AChR, by the construction of proper mutants. The present findings will be used for the rational design of the required high affinity scFv mutants.

The [G^{70}, Nle^{76}]MIR is a highly flexible oligopeptide that probably conserves only minor structural characteristics in its trajectory in the unbound state. One may also expect that the high mobility of the peptide-binding CDRs indicates an intrinsic ability of

antibodies to reduce the entropic cost of complexation upon binding of flexible loops of antigenic epitopes as in the case of [G^{70}, Nle^{76}]MIR. This illustrates the special case of flexible docking partners with dynamically "smooth" surfaces. Taking into consideration that [G^{70}, Nle^{76}]MIR has a high affinity for mAbs raised against the MIR epitope of the AChR, it is very probable that the antibody-bound peptide reflects the conformation of the parent sequence in the protein (AChR) and may prove as a valuable tool for investigating immunocomplexes in autoimmune diseases.

We thank Dr. Maigret for support. This work was supported by the Association Française contre les Myopathies, the CNRS and the HCM program of EU (grant CT94-0547), including a postdoctoral fellowship warmly acknowledged by JK.

REFERENCES

1. Tzartos, S. J.; Barkas, T.; Cung, M. T.; Mamalaki, A.; Marraud, M.; Orlewski, P.; Papanastasiou, D.; Sakarellos, C.; Sakarellos-Daitsiotis, M.; Tsantili, P.; Tsikaris, V. Immunol Rev 1998, 163, 89–120.
2. Changeux, J. P. In Fidia Research Foundation Neuroscience Award Lectures; Changeux, J. P., Llinas, R. R., Purves D., Bloom, F., Eds.; Raven Press: New York, 1990; Vol 4, pp 21–168.
3. Tzartos, S. J.; Kokla, A.; Walgrave, S.; Conti-Tronconi, B. Proc Natl Acad Sci USA 1988, 85, 2899–2903.
4. Barkas, T.; Gabriel, J.-M.; Mauron, A.; Hughes, G. J.; Roth, B.; Alliod, C.; Tzartos, S. J.; Ballivet, M. J Biol Chem 1988, 263, 5916–5925.
5. Orlewski, P.; Marraud, M.; Cung, M. T.; Tsikaris, V.; Sakarellos-Daitsiotis, M.; Sakarellos, C.; Vatzaki, E.; Tzartos, S. J. Biopolymers (Peptide Sci) 1996, 40, 419–432.
6. Bellone, M.; Tang, F.; Milius, R.; Conti-Tronconi, B. M. J Immunol 1989, 143, 3568–3579.
7. Papadouli, I.; Potamianos, S.; Hadjidakis, I.; Bairaktari, E.; Tsikaris, V.; Sakarellos, C., Cung, M. T.; Marraud, M.; Tzartos, S. J. Biochem J 1990, 269, 239–245.
8. Papadouli, I.; Sakarellos, C.; Tzartos, S. J. Eur J Biochem 1993, 211, 227–234.
9. Cung, M. T.; Tsikaris, V.; Demange, P.; Papadouli, I.; Tzartos, S. J.; Sakarellos, C.; Marraud, M. Peptide Res 1992, 5, 14–24.
10. Kabat, E. A.; Wu, T. T.; Perry, H. M.; Gottesman, K. S.; Foeller, C. In Sequences of Proteins of Immunological Interest, 5th ed; Kabat, E. A., Ed.; U.S. Department of Health and Human Services, National Institutes of Health: Bethesda, MD, 1991.
11. Chothia, C.; Lesk, A. M. J Mol Biol 1987, 196, 901–917.
12. Mariuzza, R. A.; Poljak, R. J. Curr Opin Immunol 1993, 5, 50–55.
13. Wilson, I. A.; Stansfield, R. L. Curr Opin Struct Biol 1994, 4, 857–867.
14. Chothia, C.; Lesk, A. M.; Tramontano, A.; Levitt, M.; Smith-Gill, S. J.; Air, G.; Sheriff, S.; Padlan, E. A.; Davies, D.; Tulip, W. R.; Colman, P. M.; Spinalli, S.; Alzari, P. M.; Poljak, R. J. Nature 1989, 342, 877–884.
15. Martin, A. C. R.; Cheetham, J. C.; Rees, A. R. Proc Natl Acad Sci USA 1989, 86, 9268–9272.
16. Essen, L. O.; Skerra, A. J Mol Biol 1994, 238, 226–244.
17. Chothia, C.; Lesk, A.; Levitt, M.; Amit, A.; Mariuzza, R.; Phillips, V.; Poljak, R. Science 1986, 233, 756–758.
18. De La Paz, P.; Sutton, B. J.; Darsley, M. J.; Rees, A. R. EMBO J 1986, 5, 415–425.
19. Smith-Gill, S. J.; Mainhart, C. R.; Lavoie, T. B.; Feldmann, R. J.; Drohan, W.; Brooks, B. R J Mol Biol 1987, 194, 713–724.
20. Schiweck, W.; Skerra, A. J Mol Biol 1997, 268, 934–951.
21. Moult, J.; James, M. N. G. Proteins 1986, 1, 146–163.
22. Bruccoleri, R. E.; Karplus, M. Biopolymers 1987, 26, 137–168.
23. Fine, R. M.; Wang, H.; Shenkin, P. S.; Yarmush, P. L.; Levinthal, C. Proteins 1986, 1, 342–362.
24. Mamalaki, A.; Trakas, N.; Tzartos, S. J. Eur J Immunol 1993, 23, 1839–1845.
25. Marion, D.; Ikura, M.; Tschudin, R.; Bax, A. J Magn Reson 1989, 85, 393–399.
26. Piotto, M.; Saudek, V.; Sklenar, V. J Biomol NMR 1992, 2, 661–666.
27. Sklenar, V.; Piotto, M.; Leppik, R.; Saudek, V. J Magn Reson 1993, 102A, 241–245.
28. Bartels, C.; Xia, T. H.; Billeter, M.; Güntert, P.; Wüthrich, K. J Biomol NMR 1995, 5, 1–10.
29. Maple, J. R.; Thatcher, T. S.; Dinur, U.; Hagler, A. T. Chem Design Automation News 1990, 5, 5–10.
30. Laskowski, R. A.; MacArthur, M. W.; Moss, D. S.; Thornton, J. M. J Appl Cryst 1993, 26, 283–291.
31. Güntert, P.; Berndt, K. D.; Wüthrich, K. J Biomol NMR 1993, 3, 601–606.
32. Güntert, P.; Mumenthaler, C.; Wüthrich, K. J Mol Biol 1997, 273, 283–298.
33. Fan, Z. C.; Shan, L.; Guddat, L. W.; He, X. M.; Gray, W. R.; Raison, R. L.; Edmundson, A. B. J Mol Biol 1992, 228, 188–207.
34. Fischmann, T. O.; Bentley, G. A.; Bhat, T. N.; Boulot, G.; Mariuzza, R. A.; Phillips, S. E.; Tello, D.; Poljak, R. J. J Biol Chem 1991, 266, 12915–12920.
35. Marquart, M.; Deisenhofer, J.; Huber, R.; Palm, W. J Mol Biol 1980, 141, 369–391.
36. Bernstein, F. C.; Koetzle, T. F.; Williams, G. J. B.; Meyer, E. F.; Brice, M. D.; Rodgers, J. R.; Kennard, O.; Shimanouchi, T.; Tasumi, M. J. J Mol Biol 1977, 112, 535–542.
37. INSIGHT (version 2.3.0), HOMOLOGY (version 95.0), DISCOVER (version 95.0/3.00); Biosym Technologies: 9685 Scranton Road, San Diego, CA 92121-2777, 1995.
38. Schuler, G. D.; Altschul, S. F.; Lipman, D. J. Proteins 1991, 9, 180–190.
39. Dayhoff, M. O.; Barker, W. C.; Hunt, L. T. Methods Enzymol 1983, 91, 524–545.

40. Janin, J.; Chothia, C. J Biol Chem 1990, 265, 16027–16030.
41. Hubbard, S. J.; Campbell, S. F.; Thornton, J. M. J Mol Biol 1991, 220, 507–530.
42. Goodsell, D. S.; Olson, A. J. Proteins 1990, 8, 195–202.
43. Yue, S. Protein Eng 1990, 4, 177–184.
44. Jiang, F.; Kim, S. J Mol Biol 1991, 219, 79–102.
45. Cherfils, J.; Duquerroy, S.; Janin, J. Proteins 1991, 11, 271–280.
46. Walls, P. H.; Sternberg, J. E. J Mol Biol 1992, 228, 277–297.
47. Kuntz, I. D.; Meng, E. C.; Shoichet, B. K. Acc Chem Res 1994, 27, 117–123.
48. Kozack, R. E.; Subramaniam, S. Protein Sci 1993, 2, 915–926.
49. Jones, S.; Thornton, J. M. Proc Natl Acad Sci USA 1996, 93, 13–20.
50. Chothia, C. Nature 1974, 248, 338–339.
51. Myers, J. K.; Pace, C. N.; Scholtz, M. Protein Sci 1995, 4, 2138–2148.
52. Davies, D. R.; Padlan, E. A. Annu Rev Biochem 1990, 59, 439–473.
53. Davies, D. R.; Padlan, E. A. Curr Biol 1992, 2, 254–256.
54. Stanfield, R. L.; Takmoto-Kamimura, M.; Rini, J. M.; Profy, A. T.; Wilson, I. A. Structure 1993, 1, 83–93.
55. Davies, D. R.; Cohen, G. H. Proc Natl Acad Sci USA 1996, 93, 7–12.
56. Kraulis, P. J Appl Crystallogr 1991, 24, 946–950.